A New Method For Sub-resolution Porosity Modelling On Rock Samples Using X-ray Microtomography And Pore Network Modelling Techniques

Rafael A. B. R. Alves[1], José L. D. Alves[1,2], Maira C. O. L. Santo[2], William G. A. L. da Silva[3], Elizabeth M. Pontedeiro[2], Paulo Couto[2]

[1]*Dept. of Nanotechnology Engineering, COPPE/UFRJ, Brazil*
Av. Horácio Macedo, n° 2030, Prédio do Centro de Tecnologia, sala I-127, Cidade Universitária, 21.941-972, Rio de Janeiro, Brazil
rafael.alves@coppe.ufrj.br
[2]*Dept. of Civil Engineering, COPPE/UFRJ, Brazil*
Av. Athos da Silveira Ramos, n° 149 Centro de Tecnologia, sala B-101, Cidade Universitária, 21941-909, Rio de Janeiro, Brazil
[3]*Equinor*
R. do Russel, 804 - Glória, 22210-010, Rio de Janeiro, Brazil

Abstract. The heterogeneity of carbonate rocks at multiple scales presents challenges in terms of estimating their petrophysical properties and predicting the full capacity of oil and gas reservoirs. Digital analyses are increasingly used to study the complex pore structure of carbonate rocks by means of such techniques as X-ray tomography. With this approach, one usually needs to find a compromise between the field of view (i.e., the volume dimension) and the resolution (i.e. the smallest size of distinguishable structures). For large volumes, this usually means that a fraction of the pore space, whose size is below the resolution, is not visible (i.e., the sub-resolution porosity or unresolved porosity). In this work, X-ray microtomography images of a carbonate rock with a significant fraction of porosity below the image resolution will be used to estimate flow properties. The presence of unresolved porosity is supported by mercury intrusion capillary pressure (MICP) and nuclear magnetic resonance (NMR) data. A new method is proposed for modeling the sub-resolution porosity of the images in which the topology of unresolved pores bodies/throats is correlated with the CT values of regions below the imaging resolution. Within these regions, preferential paths between visible pores will be determined using the minimal distance weighted by a probability function. Connections between visible pores are then created by assigning pore bodies and throats along these paths, whose dimensions are compatible with MICP measurements. Finally, results of numerical flow simulation with obtained pore network model are shown, demonstrating the improvement in the permeability and the potential of the proposed methodology.

Keywords: Pore network model, Sub-resolution porosity, digital rock analysis

1 Introduction

The heterogeneity of carbonate rocks at multiple scales presents a challenge in estimating petrophysical properties and predicting production of oil and gas reservoirs (Sun et al. [1]). Digital rock analysis (DRA) has been applied in the study of these systems by modelling the complex pore space based on images obtained with imaging techniques such as X-ray tomography (Micro-CT) (Godoy et al. [2], Suhrer et al. [3]) and focused ion beam scanning electron microscopy (Dvorkin et al. [4], Devarapalli et al. [5]). When applying these imaging techniques, one usually needs to find a compromise between field of view (i.e. volume dimensions) and resolution (i.e. the smallest size of distinguishable structures) (Carrillo et al. [6]). In the study of flow in porous medium, the pore space fraction whose size is below the resolution of the image can be referred to as sub-resolution porosity or unresolved porosity. This trade-off presents a special challenge on multi-modal pore systems where distinct ranges of pore sizes play a role in fluid flow and it is not possible to simultaneously image all size ranges. For a typical plug size, X-ray tomography is usually limited to resolutions of voxel size larger than 14 μm (Silveira et al. [7]).

Higher resolutions can be achieved by physically cutting a piece of the sample and scanning it (Drexler et al. [8]).

Different workflows for estimating petrophysical properties from micro-CT images have been applied. These may be divided into two main fields based on how the pore structured in modeled. The first group are based on simulation directly on the obtained segmented image or its equivalent mesh, such as Finite Elements Methods (Saxena et al. [9]) and Lattice Boltzmann (LBM) (Vogel et al. [10]). The second group, however, has an additional step to simplify the pore geometry and topology found on most natural rock, such as Pore Network Modeling (PNM) (Bultreys et al. [11]). PNM based approaches offer the benefit of reducing the computational cost to run single and multi-phase flow simulation, which in turn allows for it application on larger simulation volumes.

Regardless of the method applied for flow simulation, the potential of digital rock analysis based on these workflows is intrinsically depended on how accurately the rock porous structure can be represented by the selected imaging technique. Due to the previous discussed limitations on resolution and, consequently, how much of the pore space can be probed, additional modelling steps have been proposed to expand the descriptive ability of DRA. For instance, (Suhrer et al. [3]) and (Alves et al. [12]) proposed a approach based on correlating micro-CT attenuation with unresolved porosity and assigning petrophysical properties based on their relationships with porosity, before executing a conventional LBM simulation, in the case of the first, and FEM, for the later. For PNM based approaches, some of the proposed methods were the introduction of "micro links" (Bultreys et al. [11]) and the stochastic network generation (Jiang et al. [13]). The first approach models the unresolved porosity as pore throats ("micro links") connecting clusters of the macropore system (network extracted from the distinguishable porosity). On the other hand, Jiang et al. [13] method is based on generating a stochastic network for the micro scale (unresolved pores), which is later connected with the macro scale (resolved/distinguishable pores) via cross-scale pore throats.

The present study aims to contribute to the progress of such modelling techniques for sub-resolution porosity by developing a new approach aimed at estimating the topology of sub-resolution pores from the micro-CT images.

2 Material

As a proof of concept, one coquina core plug (sample 94.4) was selected among the four plugs characterized by Lima et al. [14]. This plug was taken from a continuous core (UFRJ 2-SMC-02-AL), drilled at Atol Quarry, located in the city of São Miguel dos Campos in the Brazilian state of Alagoas. The sample is characterized by a rock composition of 70% terrigenous, 20% bivalves and 10% cement, a interparticle pore type and sediment granulometry of fine sand (Lima et al. [14]). Plug 94.4 is an interesting candidate for sub-resolution porosity modelling because the application of PNM on its micro-CT images resulted in porosity and permeability estimations significantly lower than that measured by routine core analysis (RCAL), as presented on Table 1.

Physical Measurements			Digital Rock Analysis	
ϕ_{RCAL}	k_{RCAL}	ϕ_{NMR}	ϕ_{DRA}	k_{DRA}
18.4 %	103 mD	17.9 %	11.6 %	10.5 mD

Table 1. Lima et al. [14] reported sample 94.4 porosity (ϕ) and permeability (k) measured using routine core analysis (RCAL) and nuclear magnetic resonance (NMR), and estimated with digital rock analysis using PoreStudio for pore network modelling (DRA)

Lima et al. [14] also reported the results of mercury intrusion capillary (MICP), which was conducted for a subsample taken from an adjacent area to the drilled parts of the cores. This result is presented on Figure 1 and was integrated for the estimation of sub-resolution pore throat sizes.

Image acquisition for plug 94.4 was performed using CoreTOM equipment (Tescan/XRE) with a 14 µm voxel size, while the images were reconstructed using the Acquila reconstruction software (Tescan/XRE) (Lima et al. [14]. Threshold tools (Otsuki et al. [15]) were used to segment the image into three phases: pore, solid and "porous material" (i.e. regions expected to contain sub-resolution pores), as shown in Figure 2. Subsequently, a 1100^3 cube was cropped centered at the plug image.

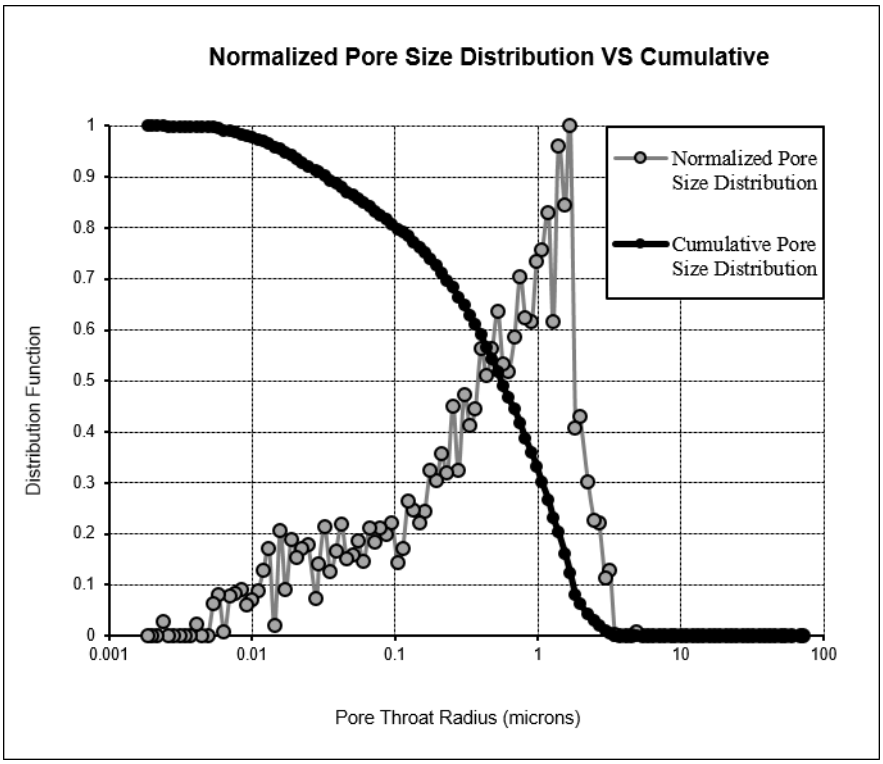

Figure 1. Pore size distribution obtained from mercury intrusion capillary pressure experiment for sample 94.4 (Lima et al. [14])

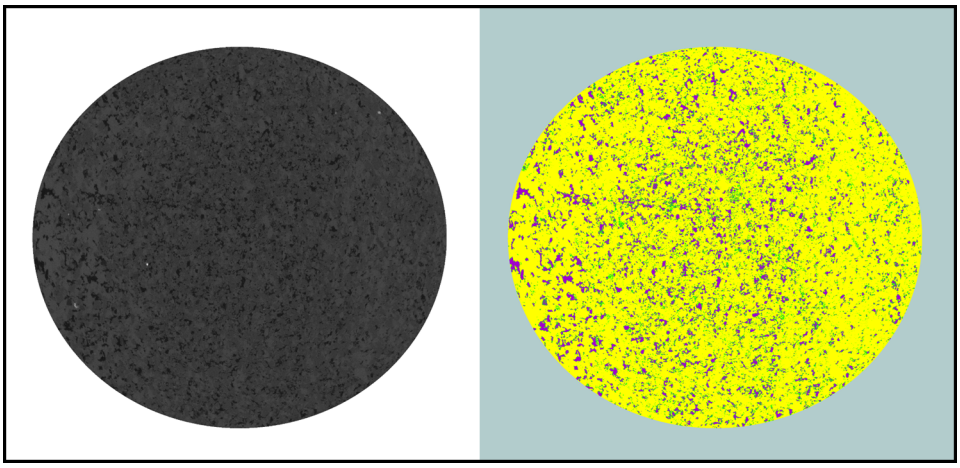

Figure 2. On the left, cross section of X-ray tomography for sample 94.4 plug. On the right, segmentation of image in three phases: pore (purple), solid (yellow) and sub-resolution porous material (green).

3 Methodology

The workflow proposed in this paper starts with the segmentation of the micro-CT image into three phases: solid, pore and unresolved porous material. A pore network model is extracted for the segmented pore phase, obtaining a "macropore network" which characterizes the pore space within the image resolution. For sample 94.4, this step was done using PoreSpy (Gostick et al. [16]), an open source pore network extraction software.

On the macropore network, disconnected pore systems (i.e. clusters) are identified and assigned a label, which is then mapped to their respective voxels of the segmented volume. The resulting grid will be named "labeled connectivity map" from here on. In the selected sample crop, the largest cluster is also the one responsible for the overall connectivity, and will be referred to as "main cluster". The labeled connectivity map and the segmented unresolved pore phase are superimposed and a binary connected components labeling algorithm is executed to

identify which clusters are connectable with the main cluster through the unresolved phase. Identified clusters will be candidates for connection through the sub-resolution network and are named "connectable clusters". In this work, we used the open source software "cc3d" (Silversmith [17]) to complete this task.

For each pair of main and connectable clusters, the distance between their pore bodies centers is computed. The objectives of this step are to estimate the proximity of the clusters and to identify the closest pairs of pore bodies. Clusters and pores geometrically closer to each other are assumed to be more likely to be connected by sub-resolution porosity, thus guiding the decision of which clusters should be connected by the sub-resolution network created later on this workflow. A more precise computation of these distance can be obtained by considering the surface voxels forming the clusters, instead of the simplified network description. However, this approach is significantly more computationally intense and was not pursued.

A fraction of the closest pore body pairs are then selected to be starting and ending points (i.e. "sources" and "targets") for the sub-resolution network. A smaller volume around these pore body pairs is selected keeping a segmented sub-resolution porous phase connecting both elements. This volume is referred to as "pathing volume" and its selection is done to reduce the computational load on subsequent computations. To avoid limiting sources and targets to just the two selected pore bodies, different voxels on the surface of their respective clusters are used instead. This means that the obtained path may connect different pore bodies from the one used to define the pathing volume, however this is not an issue as the objective of this procedure is to connect the clusters and not specifically the two pore bodies selected. This also has the benefit of increasing the pool of available macropores for connections.

A "weight" is assigned to each voxel within the pathing volume based on its respective value on the segmentation and scan images. This weight is an empirical representation of the probability of the voxel not containing sub-resolution porosity, i.e. a larger weight means a lower probability of sub-resolution pores being present. An arbitrary near zero and an arbitrary large (much larger than 1) weight is assigned to segmented pore and solid phases, respectively. For the unresolved pore phase, a value between 0 and 1 is assigned based on the normalized CT value of the scan image, meaning that lower CT values result in lower weights and higher probability of sub-resolution porosity.

Within the pathing volume, the sequence of voxels which connect the source and target pores with the lowest associated weight (i.e. the "shortest weighted path") is determined. The minimum distance algorithm selected for this task was the open source "dijkstra3d" (Silversmith [18]), which offers an implementation of Dijkstra [19] algorithm optimized for 3D image volumes.

Finally, the sub-resolution network is generated within the voxels of the shortest weighted path and its extremities are connected to the source/target pore bodies associated to the source/target voxel of the macropore network, thus obtaining a final pore network where the previously disconnected clusters are now connected through the sub-resolution porosity. To create such structure, first a group of throat lengths is generated according to a normal distribution, centered at the mean length of the entire path, truncated at a lower limit and upper limit of 10% and 30% of the total length of the path, respectively. Alternatively, one can use the throat length distribution of the macropore network itself. These pore throats will be used to connect the macropore bodies and the generated sub-resolution pore bodies sequentially. This means that the centers of the new pore bodies are positioned between these pore throats, which are oriented along the shortest weighed path. Pore throat radii are then assigned based on the MICP pore size distribution, taking just he part bellow the voxel resolution. Pore bodies radii are then determined by a shifted throat radius distribution and are selected to always be larger than its connecting throat radii, to preserve the expected opening/closing sequence which defined pore bodies and throats.

Once this procedure is completed, porosity and absolute permeability can be computed for the obtained network using the same tools as the conventional macropore network.

4 Results and conclusions

The macropore network extracted for sample 94.4 has 128,967 disconnected clusters, with the number of pore bodies ranging from a single pore to 1,738 (excluding the main cluster). The main cluster, responsible for the sample overall connectivity from top to bottom, has 210,788 pore bodies. Total and connected porosity was later computed trough voxel counting of the segmented image and prediction of absolute permeability was obtained using OpenPNM (Gostick et al. [20]), both results are presented on Table 2.

The sub-resolution network was generated to connect the main cluster with the six largest "connectable clusters" (6 pairs). For each pair, the 50 closest pore bodies were used as a base for the pathing volume, on which 11 target-source pairs were selected, resulting in a total of 3300 "paths" of sub-resolution pore bodies and throats being generated and integrated to the macropore network. In total, the number of pore bodies and pore throats in the final network was approx. 3.61 % and 4.37 % larger than in the macropore network, respectively.

This modification translates to a neglectable total porosity increase of approx. 0.002 %, due to the small size

Total Porosity	Connected Porosity	Absolute Permeability
9.3299 %	5.8816 %	20.98 mD

Table 2. Porosity and permeability estimation for extracted pore network model, including only the pore space captured at the scan resolution.

and number of additional sub-resolution pore elements, a small connected porosity increase of approx. 1.8 %, mainly due to the connection of previous disconnected clusters, and an increase of permeability from 20.98 mD to 29.15 mD (approx. 39 % increase). These results are summarized on Table 3.

Total Porosity	Connected Porosity	Absolute Permeability
9.3301 %	5.9889 %	29.15 mD

Table 3. Porosity and permeability estimation for extracted pore network model after inclusion of a small fraction of sub-resolution porosity.

The results for the obtained network represent a first attempt of the proposed methodology, with a limited inclusion of sub-resolution porosity, as observed by the small increase in total porosity. The significant improvement in permeability, however, demonstrates the importance of sub-resolution pores to the overall flow in the sample and indicates the potential of the proposed method.

Although these digital estimations are still not comparable with physical measurements, it is important to notice that the procedure could be applied to a larger extend to create more sub-resolution networks and/or connect more clusters, thus potentially resulting in a more representative network.

Additionally, modifications in the procedure could also improve results. Regarding the creation of sub-resolution network within the selected "voxel paths", improvements can be made by replacing the sequential connections by a more realistic topology, or creating connecting structures among sub-resolution paths. Another promising approach is to obtain a more even distribution of the generated network along the surface of the main cluster, instead of concentrating on just a few of the closest regions.

The proposed workflow shows potential to improve pore network modelling estimations for samples whose scans are insufficient to capture the relevant part of the pore space. At the same time, the presented proof of concept using a coquina sample demonstrates the importance that sub-resolution porosity may play on the determination of representative petrophysical properties through digital rock analysis.

Acknowledgements. Rafael A. B. R. Alves acknowledges the support of the Program of Nanotechnology Engineering (PENt-COPPE/UFRJ) in this research. José L. D. Alves, Maira C. O. L. Santo, Elizabeth M. Pontedeiro e Paulo Couto gratefully acknowledge the partial support of Shell in this research, which is associated with the ongoing R&D project registered as ANP nº 23020-1, "Caracterização Experimental, Modelagem e Otimização de Processos de Injeção de Água Alternada Com Gás – WAG-EX Fase II" (UFRJ/Shell Brasil/ANP), sponsored by Shell Brasil Petróleo Ltda under the ANP R&D levy as "Compromisso de Investimentos com Pesquisa e Desenvolvimento".

Authorship statement. The authors hereby confirm that they are the sole liable persons responsible for the authorship of this work, and that all material that has been herein included as part of the present paper is either the property (and authorship) of the authors, or has the permission of the owners to be included here.

References

[1] H. Sun, S. Vega, and G. Tao. Analysis of heterogeneity and permeability anisotropy in carbonate rock samples using digital rock physics. *Journal of petroleum science and engineering*, vol. 156, pp. 419–429, 2017.

[2] W. Godoy, E. M. Pontedeiro, F. Hoerlle, A. Raoof, M. T. Van Genuchten, J. Santiago, P. Couto, and others. Computational and experimental pore-scale studies of a carbonate rock sample. *Journal of Hydrology and Hydromechanics*, vol. 67, n. 4, pp. 372–383, 2019.

[3] M. Suhrer, X. Nie, J. Toelke, and S. Ma. Upscaling method for obtaining primary drainage capillary pressure and resistivity index with digital rock physics. In *International Petroleum Technology Conference*, pp. D033S066R003. IPTC, 2020.

[4] J. Dvorkin, N. Derzhi, E. Diaz, and Q. Fang. Relevance of computational rock physics. *Geophysics*, vol. 76, n. 5, pp. E141–E153, 2011.
[5] R. S. Devarapalli, A. Islam, T. F. Faisal, M. Sassi, and M. Jouiad. Micro-ct and fib–sem imaging and pore structure characterization of dolomite rock at multiple scales. *Arabian Journal of Geosciences*, vol. 10, pp. 1–12, 2017.
[6] F. J. Carrillo, C. Soulaine, and I. C. Bourg. The impact of sub-resolution porosity on numerical simulations of multiphase flow. *Advances in Water Resources*, vol. 161, pp. 104094, 2022.
[7] T. M. Silveira, F. Hoerlle, A. S. Rocha, M. C. Lima, M. G. Ramirez, E. M. Pontedeiro, M. T. Van Genuchten, D. O. Cruz, P. Couto, and others. Effects of carbonated water injection on the pore system of a carbonate rock (coquina). *Journal of Hydrology and Hydromechanics*, vol. 70, n. 2, pp. 257–268, 2022.
[8] S. Drexler, R. Bastos Alves, V. Silos, M. Ferreira De Siqueira, and J. Toelke. New method to simulate digital petrophysical properties in heterogeneous carbonates using multiscale micro computed tomography imaging and customized laboratory experiments. In *International Petroleum Technology Conference*, pp. D012S124R003. IPTC, 2022.
[9] N. Saxena, R. Hofmann, F. O. Alpak, S. Berg, J. Dietderich, U. Agarwal, K. Tandon, S. Hunter, J. Freeman, and O. B. Wilson. References and benchmarks for pore-scale flow simulated using micro-ct images of porous media and digital rocks. *Advances in Water Resources*, vol. 109, pp. 211–235, 2017.
[10] H.-J. Vogel, J. Tolke, V. Schulz, M. Krafczyk, and K. Roth. Comparison of a lattice-boltzmann model, a full-morphology model, and a pore network model for determining capillary pressure–saturation relationships. *Vadose Zone Journal*, vol. 4, n. 2, pp. 380–388, 2005.
[11] T. Bultreys, L. Van Hoorebeke, and V. Cnudde. Simulating secondary waterflooding in heterogeneous rocks with variable wettability using an image-based, multiscale pore network model. *Water Resources Research*, vol. 52, n. 9, pp. 6833–6850, 2016.
[12] R. Alves, S. Drexler, B. Silva, V. Silos, J. Toelke, and M. Siqueira. Elastic properties upscale for carbonate rocks using finite element numerical modeling and differential effective medium theory. In *First EAGE Rock Physics Workshop in Latin America*, number 1, pp. 1–5. European Association of Geoscientists & Engineers, 2021.
[13] Z. Jiang, M. Van Dijke, K. S. Sorbie, and G. D. Couples. Representation of multiscale heterogeneity via multiscale pore networks. *Water resources research*, vol. 49, n. 9, pp. 5437–5449, 2013.
[14] M. C. Lima, E. M. Pontedeiro, M. G. Ramirez, J. Favoreto, dos H. N. Santos, van M. T. Genuchten, L. Borghi, P. Couto, and A. Raoof. Impacts of mineralogy on petrophysical properties. *Transport in Porous Media*, vol. 145, n. 1, pp. 103–125, 2022.
[15] B. Otsuki, M. Takemoto, S. Fujibayashi, M. Neo, T. Kokubo, and T. Nakamura. Pore throat size and connectivity determine bone and tissue ingrowth into porous implants: three-dimensional micro-ct based structural analyses of porous bioactive titanium implants. *Biomaterials*, vol. 27, n. 35, pp. 5892–5900, 2006.
[16] J. T. Gostick, Z. A. Khan, T. G. Tranter, M. D. Kok, M. Agnaou, M. Sadeghi, and R. Jervis. Porespy: A python toolkit for quantitative analysis of porous media images. *Journal of Open Source Software*, vol. 4, n. 37, pp. 1296, 2019.
[17] W. Silversmith. seung-lab/connected-components-3d: Zenodo Release v1, 2021.
[18] W. Silversmith. seung-lab/dijkstra3d, 2023.
[19] E. W. Dijkstra. A note on two problems in connexion with graphs. *Numerische Mathematik*, vol. 1, pp. 269–271, 1959.
[20] J. Gostick, M. Aghighi, J. Hinebaugh, T. Tranter, M. A. Hoeh, H. Day, B. Spellacy, M. H. Sharqawy, A. Bazylak, A. Burns, and others. Openpnm: a pore network modeling package. *Computing in Science & Engineering*, vol. 18, n. 4, pp. 60–74, 2016.